

Sparse Reconstruction of Breast MRI using Homotopic L_0 Minimization in a Regional Sparsified Domain

Alexander Wong, *Member, IEEE*, Akshaya Mishra, *Member, IEEE*, Paul Fieguth, *Member, IEEE*, and David A. Clausi, *Member, IEEE*

Abstract—The use of magnetic resonance imaging (MRI) for early breast examination and screening of asymptomatic women has become increasingly popular, given its ability to provide detailed tissue characteristics that cannot be obtained using other imaging modalities such as mammography and ultrasound. Recent application-oriented developments in compressed sensing theory have shown that certain types of magnetic resonance images are inherently sparse in particular transform domains, and as such can be reconstructed with a high level of accuracy from highly undersampled k-space data below Nyquist sampling rates using homotopic L_0 minimization schemes, which holds great potential for significantly reducing acquisition time. An important consideration in the use of such homotopic L_0 minimization schemes is the choice of sparsifying transform. In this work, a regional differential sparsifying transform is investigated for use within a homotopic L_0 minimization framework for reconstructing breast MRI. By taking local regional characteristics into account, the regional differential sparsifying transform can better account for signal variations and fine details that are characteristic of breast MRI than the popular finite differential transform, while still maintaining strong structure fidelity. Experimental results show that good breast MRI reconstruction accuracy can be achieved compared to existing methods.

Index Terms—MRI, magnetic resonance imaging, reconstruction, minimization, regional differential transform, breast

I. INTRODUCTION

Based on statistics collected by the World Health Organization International Agency for Research on Cancer, breast cancer has become the most frequently occurring form of cancer found in women worldwide, with an estimated 636,000 incidents in developed countries and 514,000 incidents in developing countries in 2002 [1]. Of greater concern is the related fact that breast cancer has also become the most prominent cause of cancer-related deaths in women in many countries, with an estimated 519,000 deaths worldwide in 2004 [2], due partly to the increased risk of developing a second primary cancer along with the breast cancer [3]. To date, the most effective way to reduce the breast cancer related mortality is through early breast screening of asymptomatic women to identify possible signs of breast abnormalities. Early detection of breast cancer can allow for early-stage treatments that can significantly improve breast cancer survival rates while reducing treatment complications [4].

The most widely used imaging technology for breast screening in the past four decades is mammography, where breast X-ray images are acquired to aid in the detection of breast tissue abnormalities such as masses and microcalcifications.

While the use of mammography for breast cancer screening is widely available and has been shown to allow for reliable identification and detection of calcifications, there are a number of limitations. First, the mammography procedure requires the compression of breast tissue for proper imaging, leading to both patient anxiety and discomfort. This discomfort is amplified by the fact that the breast must be repositioned to allow for different views to be acquired. Second, due to the way x-ray imaging functions, abnormalities in dense breast tissue can be more difficult to detect using mammography. This is particularly problematic when screening young women, who usually have denser breasts than older women. Third, the mammography procedure requires exposure to harmful ionizing radiation, which can lead to potential harm to the patient. In recent years, the use of magnetic resonance imaging (MRI) for early breast examination and screening of asymptomatic women has become increasingly established as a complementary tool to mammography for studying breast cancer, where abnormalities identified using mammography are studied in detail using breast MRI. There are a number of important advantages to the use of breast MRI for breast cancer screening. First, due to the higher tissue sensitivity in MRI when compared to mammography, breast MRI allows for easier identification and detection of fine-scale signs of breast tissue abnormalities, particularly in dense breast tissue. Second, no compression of the breast tissue is required, and both breasts are imaged simultaneously to create volumetric breast tissue data, hence potentially reducing some of the patient discomfort associated with mammography. Third, unlike mammography, MRI does not expose patients to ionizing radiation.

Despite the advantages associated with MRI for breast cancer screening, a main limitation with this approach is the long acquisition time, which can contribute to patient discomfort, as well as limiting the number of screenings that can be done. For example, in the case of fast dynamic contrast-enhanced breast MRI [5], [6], within a session, a pre-contrast acquisition is followed by multiple post-contrast acquisitions after contrast injection. This type of breast MRI acquisition allows for the observation of contrast uptake over time, which can be potentially used to differentiate between malignant tumors and benign lesions. In the case of 2.0mm slice thickness and 18cm range of coverage and a 0.5mm gap, and a total of 1 pre-contrast and 5 post-contrast acquisitions at 1 minute increments within the session, the total of number

slices acquired is approximately 432 slices. Given a time of repetition (TR) of 4.6ms and 420 TRs per slice, could have an approximate acquisition time of 14.5 minutes. Early attempts at reducing acquisition times such as echo-planar imaging [7] come at the cost of high hardware complexity and low signal-to-noise ratios, as well as the presence of distortions due to factors such as eddy currents and off-resonance effects. Additionally, breast MRI data are often acquired using a coil array, which can also be used for accelerated acquisition. To address the issue associated with long acquisition times without increasing hardware complexity or sacrificing significant signal-to-noise ratios, recent developments in compressed sensing theory [8], [9] with respect to medical imaging have shown that certain types of magnetic resonance (MR) images can be reconstructed with a high level of accuracy from highly undersampled k-space data below Nyquist sampling rates, hence significantly reducing acquisition time [10].

Given the significant benefits that can be gained, a wide variety of reconstruction approaches have been proposed for the purpose of MRI reconstruction [10], [11], [12], [13], [14], [15], [16], [17], [18], [19], [20], [21], [34]. In particular, a homotopic L_0 minimization approach [20] was shown to provide superior reconstruction for spine and wrist MRI from significantly undersampled k-space data when compared to state-of-the-art methods [21]. The ability to achieve highly accurate reconstructions from highly undersampled k-space data is very important in reducing acquisition time, since the acquisition time is proportional to the number of k-space lines acquired [10]. However, the effectiveness of such an approach for breast MRI reconstruction has not been explored, and may not be well-suited given its use of the finite differential transform, which is poorly suited for handling the fine details and variations found in breast MRI. More recently, Liang et al. [14] explored the use of the non-local total variation regularization framework [22], [23] for MRI reconstruction, where regional characteristics between non-local sites from throughout the data is used as a penalty constraint, and found that such an approach allowed for improved handling of fine details and variations. However, once again, the effectiveness of such an approach for breast MRI reconstruction, particularly within a homotopic L_0 minimization framework, has not been explored in previous literature. Furthermore, by considering non-local sites in the optimization process, the computational complexity for reconstruction can be relatively high. As such, exploring a graceful compromise between the local finite differential transform and the non-local total variation approach is desired.

In this work, the concept of a regional differential sparsifying transform is investigated for use within a homotopic L_0 minimization framework for improving the reconstruction of breast MRI. By extending the finite differential transform to take local regional characteristics into account, the regional differential sparsifying transform can better account for signal variations and fine details that are characteristic of breast MRI like the non-local total variation approach than the popular finite differential transform, while still maintaining strong structure fidelity. Furthermore, by remaining a local transform like the finite differential transform, the computational complexity for reconstruction is lower than the non-local

total variation approach. Interestingly, the proposed regional differential sparsifying transform can be viewed as a special case of the non-local total variation approach.

The proposed work makes two main contributions. First, to the best of the authors' knowledge, this is the first time where different sparsifying transforms are explored for the suitability of sparse breast MRI reconstruction. Second, this is the first time such a regional differential sparsifying approach has been investigated for sparse breast MRI reconstruction. The theory behind homotopic L_0 minimization using a regional differential sparsifying transform for breast MRI reconstruction is introduced in Section II. Experimental results are presented and discussed in Section III. Finally, conclusions are drawn and future work is discussed in Section IV.

II. THEORY

A. L_p minimization for sparse reconstruction

Let S be set of sites in a discrete lattice \mathbb{L} upon which an MRI image is defined in the spatial domain and $s \in S$ be a site in \mathbb{L} . Let K be a set of sites in a discrete spectral lattice \mathbb{F} upon which the same MRI image is defined in k-space and $k \in K$ be a site in \mathbb{F} . Given that all measurements are made in k-space for MRI, the relationship between the signal $F(k)$ in k-space and the equivalent signal $f(s)$ in the spatial domain can be expressed as,

$$f(s) = \mathcal{F}^{-1} \Phi F(k), \quad (1)$$

where \mathcal{F}^{-1} is the inverse Fourier operator and Φ is a measurement operator defining which sites in K are measured (Φ assigns zeroes to non-measured k-space indices). As such, the reconstruction of $f(s)$ from $F(k)$ is essentially an inverse problem. In the case where Φ is not the identity matrix, such as when fewer measurements are made to reduce acquisition time, not all sites in K are measured, making the inverse problem underdetermined with multiple solutions. Traditionally, this inverse problem is solved via a constrained L_2 minimization in the spatial domain, as expressed by,

$$\hat{f}(s) = \arg \min_{f(s)} \|f(s)\|_2 \quad s.t. \quad \Phi \hat{F}(k) = \Phi F(k). \quad (2)$$

where $\hat{f}(s)$ and $\hat{F}(k)$ are estimated signals in the spatial and k-space domains. However, solving the problem in this manner results in significant artifacts such as aliasing and temporal blurring in practical situations [21].

Recently, scientists realized that many signals, such as MR images, possess inherent sparsity in some sparsifying transform Ψ , and that a significantly better estimate of $f(s)$ can be obtained by maximizing sparsity in Ψ while enforcing data fidelity in K . As a result, this can be formulated as a constrained L_0 minimization problem in Ψ , subject to data fidelity constraints in K ,

$$\hat{f}(s) = \arg \min_{f(s)} \|\Psi f(s)\|_0 \quad s.t. \quad \Phi \hat{F}(k) = \Phi F(k). \quad (3)$$

Unfortunately, solving the constrained L_0 minimization problem in Ψ is non-deterministic polynomial-time hard (NP-hard) and intractable in practical situations. To work around this computational complexity problem, the breakthrough work by

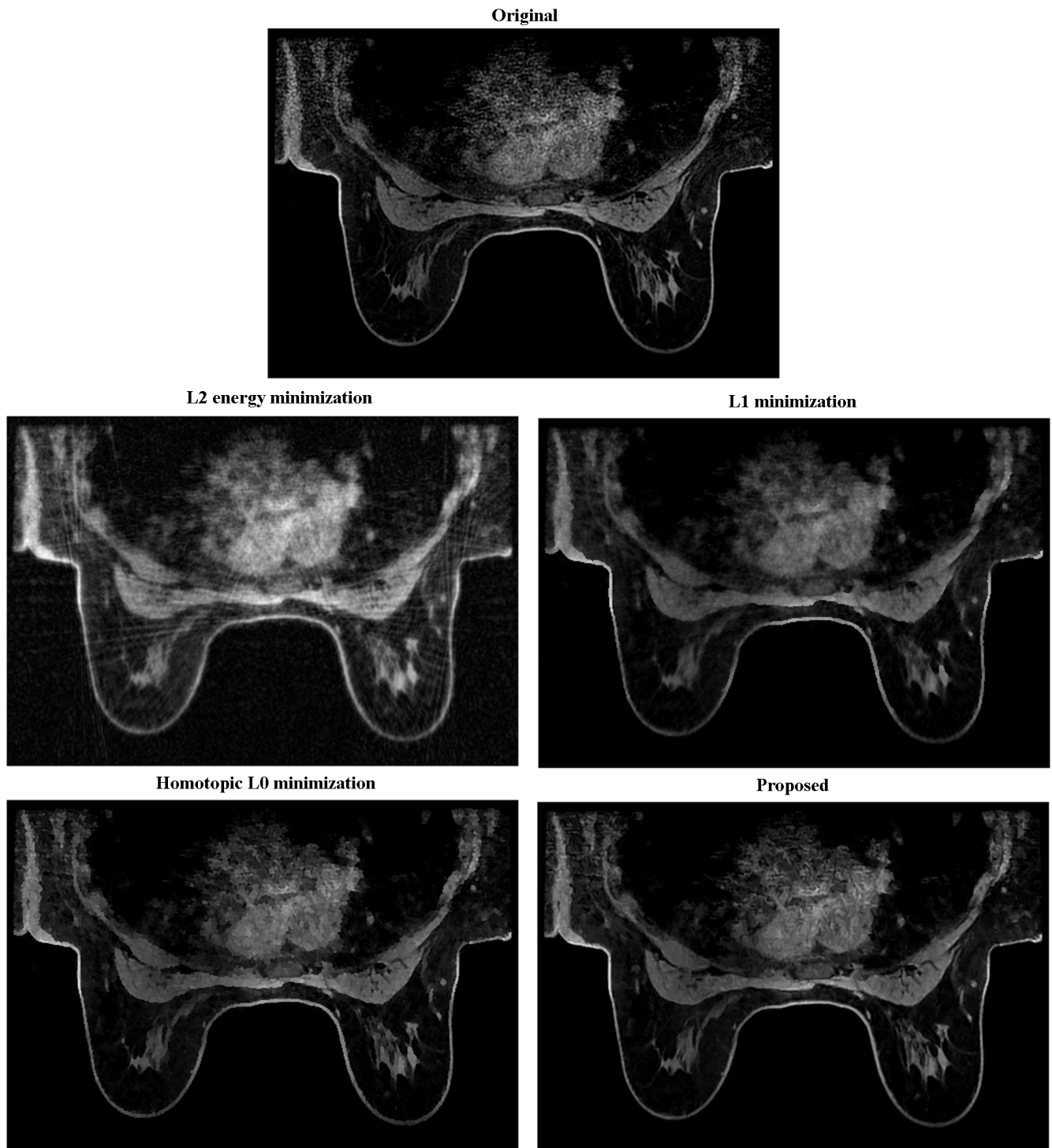


Fig. 1. Sample reconstructions using the tested breast MRI reconstruction methods (83% undersampling). Note that the reconstructions have been cropped for display purposes, resulting in non-square dimensions.

Candés et al. [8], as well as work by Donoho [9], showed that the use of L_1 norm can still yield perfect reconstructions at the cost of increased measurements,

$$\hat{f}(s) = \arg \min_{f(s)} \|\Psi f(s)\|_1 \quad s.t. \quad \Phi \hat{F}(k) = \Phi F(k). \quad (4)$$

The constrained L_1 minimization problem is convex and tractable in practical situations, and as such has become the basis for much of the work on sparse reconstruction since that seminal work, some of which include [8], [9], [10], [11], [12], [15]. However, from a theoretical perspective, the constrained L_1 minimization problem may require a drastic increase in the number of measurements needed to achieve the same results as the constrained L_0 minimization problem, based on the theoretical L_0 requirements.

To get closer to the theoretical capabilities of the constrained L_0 minimization problem, Trzasko and Manduca [21] introduced a new reconstruction paradigm called homotopic L_0 minimization, where an increasingly stronger approximation of the L_0 minimization problem is used to iteratively reconstruct $f(s)$ [21],

$$\hat{f}(s) = \lim_{\sigma \rightarrow 0} \arg \min_{f(s)} \sum_S \rho(|\Psi f(s)|, \sigma) \quad s.t. \quad \Phi \hat{F}(k) = \Phi F(k). \quad (5)$$

where ρ is a homotopic approximate of the L_0 norm that moves closer to the true L_0 norm as the approximate L_0 relaxation term $\sigma \in \mathfrak{R}$ approaches 0. In many cases, quasi-convex functions such as the Geman-McClure [25] functions are chosen for the homotopic approximate of the L_0 norm. The advantage of this approach is many-fold, as it is able to identify the local minima of the cost function with roughly the same complexity as the L_1 minimization approach, while better approaching the theoretical capabilities of the constrained L_0 minimization approach. To account for noise in the measured values, the data fidelity constraint is typically replaced by an L_2 norm constraint, leading to the final formulation

$$\begin{aligned} \hat{f}(s) = \lim_{\sigma \rightarrow 0} \arg \min_{f(s)} \sum_S \rho(|\Psi f(s)|, \sigma) \\ s.t. \quad \left\| \Phi \hat{F}(k) - \Phi F(k) \right\|_2 < \epsilon, \end{aligned} \quad (6)$$

where ϵ is an error bound.

B. Regional differential sparsifying transform for breast MRI reconstruction

An important issue that is worth investigating with regards to the homotopic L_0 minimization approach is the choice of sparsifying transform domain Ψ . The choice of Ψ is critical in obtaining good reconstructions, as the underlying premise is that the signal is highly sparse in the sparsifying transform domain. Two popular choices for sparsifying transforms are the finite differential transform and the wavelet transform [10]. The finite differential transform is a popular choice particularly in reconstruction strategies based on total variational models [26], such as that used in the original homotopic L_0 minimization approach. The finite differential transform is highly sparse for piece-wise constant scenarios, but considerably less sparse in more complex scenarios characterized

by fine details and non-uniform signal variations. Since breast MRI is characterized by fine details and signal variations due to the underlying tissue characteristics, particularly pertaining to suspicious tissue anomalies such as masses and microcalcifications, the finite differential transform is not well-suited for reconstructing such data. Furthermore, a common artifact in reconstructions using finite differential transform is the staircase effect, which has the potential to degrade the quality of clinical diagnosis using such reconstructions. The wavelet transform can better handle fine details and signal variations but at the cost of reduced structure fidelity [21], which is important for morphological studies of suspicious cancer-related abnormalities such as masses and microcalcifications.

To tackle the issue associated with handling fine detail and signal variations faced by the finite differential transform while maintaining strong structure fidelity, we investigate the concept of the regional differential sparsifying transform, where local regional characteristics are taken into account in the differential formulation. Let a neighboring site of s , denoted as s_j , be a site that is within a common fifth-order Markov connectivity with s . Let the regional differential sparsifying transform between a site s and a neighboring site s_j be defined by

$$\Psi_R(s, s_j) = \sum_{l \in R} |f(s+l) - f(s_j+l)| \quad (7)$$

where l is the set of indices defining an equal-sized region around each site. By taking local regional characteristics into account, the regional differential transform can better account for signal variations and fine details, which are important for breast MRI reconstruction, while still maintaining strong structure fidelity such as the finite differential transform.

Based on Eq. 7, the homotopic L_0 norm for the sparse representation in the regional differential sparsifying transform domain can be defined as

$$\|\Psi_R f(s)\|_0 = \lim_{\sigma \rightarrow 0} \sum_{s \in S} \sum_{n \in \Omega} \rho(\Psi_R(s, s+n), \sigma) \quad (8)$$

where Ω denotes the set of all sites within a fifth-order Markov connectivity around s . The proposed regional differential sparsifying transform shares similarities with the non-local total variation regularization framework [22], [23] that was employed by Liang et al. [14] for MRI reconstruction, which takes advantage of regional characteristics between non-local sites from throughout the data for regularization purposes. However, the proposed regional differential sparsifying transform differs from the non-local total variation approach in that, like the finite differential sparsifying transform it is extending upon, only close neighboring sites are used in computing the transform and hence is a local transform. As such, the proposed regional differential sparsifying transform can be viewed as a special case of the non-local total variation approach where only close neighboring sites are used with a uniform weighting scheme. This type of approach can be viewed as a ‘‘semi-local’’ approach [24]. Therefore, the computational complexity of the regional differential sparsifying transform is reduced when compared to the standard non-local total variation approach yet still reaping the benefits of using local

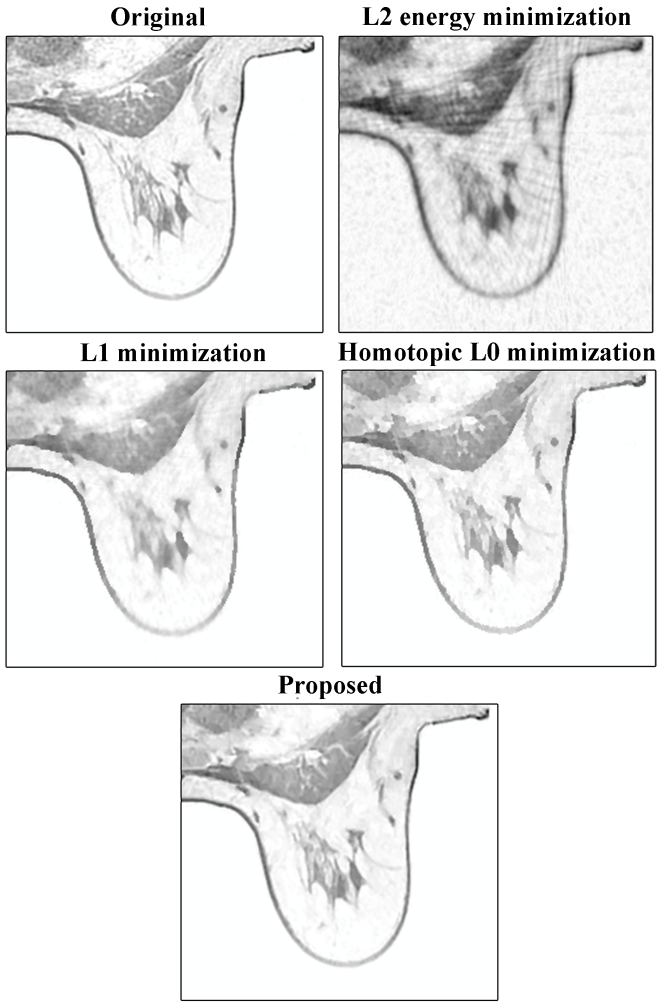


Fig. 2. Inverted zoomed-in regions from the sample reconstructions using the tested breast MRI reconstruction methods.

regional characteristics, hence providing a graceful compromise between the finite differential sparsifying transform and the non-local total variation approach.

Based on Eq. 6 and Eq. 8, the final homotopic L_0 minimization in the regional differential sparsifying domain can thus be expressed by

$$\hat{f}(s) = \lim_{\sigma \rightarrow 0} \arg \min_{f(s)} \sum_S \rho(|\Psi_R f(s)|, \sigma) \quad (9)$$

$$s.t. \quad \left\| \Phi \hat{F}(k) - \Phi F(k) \right\|_2 < \epsilon.$$

Given the problem formulation shown in Eq. 9, an objective function Υ can be defined as

$$\Upsilon(\hat{f}(s), \sigma, \lambda) = \sum_S \rho(|\Psi_R \hat{f}(s)|, \sigma) + \lambda \left\| \Phi \hat{F}(k) - \Phi F(k) \right\|_2 \quad (10)$$

where λ is a data fidelity relaxation constant that controls the contribution of the data fidelity constraint compared to the approximate L_0 sparsity constraint. Since MRI data is complex in nature, Eq. 10 can be modified to penalize sparsity for both

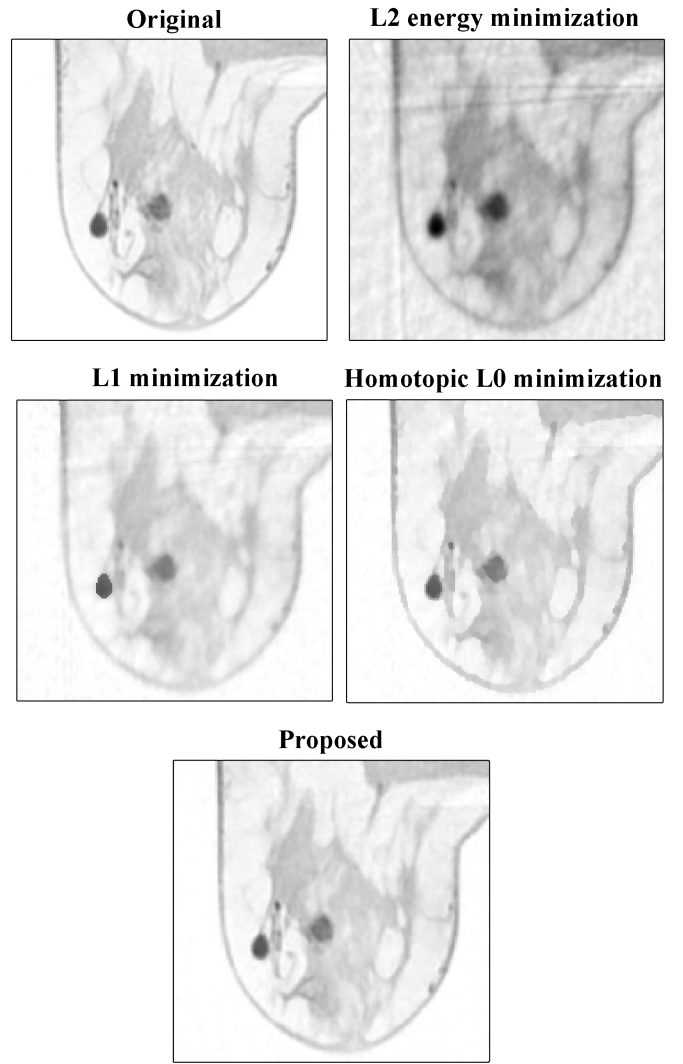


Fig. 4. Inverted zoomed-in regions from the second set of sample reconstructions using the tested breast MRI reconstruction methods.

the real and imaginary components of the data,

$$\Upsilon(\hat{f}(s), \sigma, \lambda) = \sum_S \rho(|\Psi_R \Re\{\hat{f}(s)\}|, \sigma) + \sum_S \rho(|\Psi_R \Im\{\hat{f}(s)\}|, \sigma) + \lambda \left\| \Phi \hat{F}(k) - \Phi F(k) \right\|_2. \quad (11)$$

III. EXPERIMENTAL RESULTS

The proposed approach was evaluated using T1-weighted breast MRI data acquired at St. John's Mercy to investigate its potential for sparse breast MRI reconstructions from highly undersampled k-space data below Nyquist sampling rates. The MRI machine used to acquire the breast MRI was a GE Signa HDx 1.5T MRI system with SMI high performance variable geometry coils, set to a repetition time (TR) of 4.60ms and an echo time (TE) of 2.20ms. The three sets of tested breast MRI data sets consist of 512×512 16-bit data with a displayed field of view (DFOV) of $30.0\text{cm} \times 30.0\text{cm}$ and 2.0mm thickness.

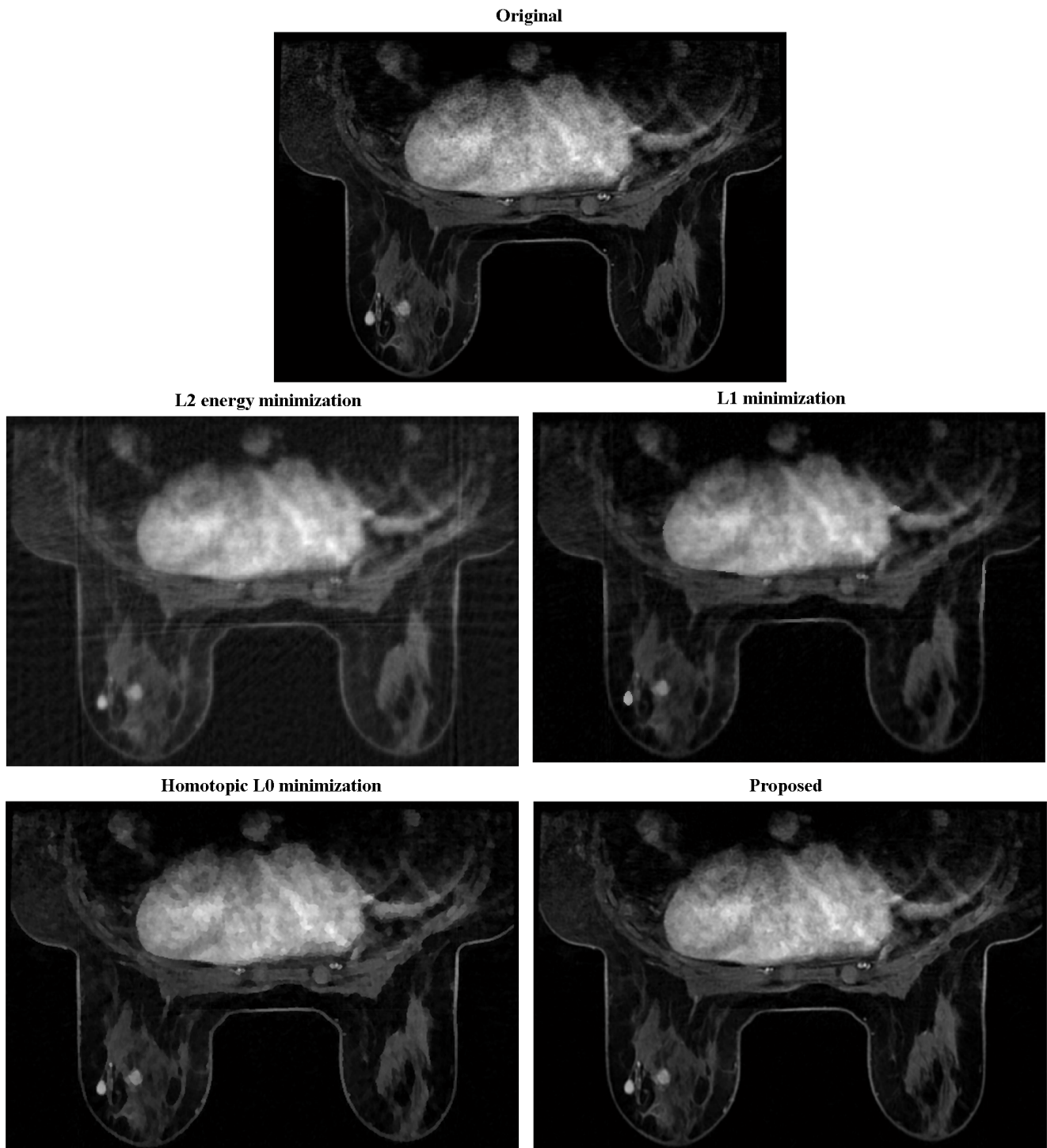


Fig. 3. Second set of sample reconstructions using the tested breast MRI reconstruction methods (83% undersampling). Note that the reconstructions have been cropped for display purposes, resulting in non-square dimensions.

Although the available data is real-valued, there are a number of ways to deal with the issue of phase in complex-valued data that have been thoroughly explored in related work. For example, if the data is dominantly real, phase correction approaches such as homodyne detection [35] can be employed during reconstruction process [10]. Furthermore, the study by Trzasko and Manduca [21] showed that, despite the typical scenario of smoothly varying phase, accurate reconstructions can be achieved even at significant k-space undersampling for data where phase information is less dominant, such as breast MRI where phase also seldom provide diagnostic information [27].

To test the effectiveness of the proposed reconstruction approach, breast MRI reconstructions were produced based on radial k-space sampling trajectories at 83% k-space undersampling. The use of radial k-space sampling trajectories have become increasingly popular in practice for breast MRI, given its lower susceptibility to motion artifacts than standard Cartesian k-space sampling trajectories [29], and has been shown for other types of MRI data to allow for significant k-space undersampling [30]. Therefore, the use of radial k-space sampling trajectories is well-suited for our tests. Note that, for simulation purposes, Cartesian approximations of the radial k-space sampling trajectories were used given the available data. In more real-world situations using actual radial data, re-gridding approaches such as the well-known Kaiser-Bessel gridding approach [31] and non-uniform fast Fourier transform (NUFFT)-based gridding approaches [32] can be incorporated into the proposed approach to interpolate radial data onto a Cartesian coordinate system for subsequent reconstruction.

For comparison purposes, the proposed approach is compared to three other published techniques: the baseline L_2 energy minimization approach, the classic L_1 minimization approach proposed by Lustig et al. [10] that simultaneously promotes transform domain sparsity and penalizes total variation norm, and the homotopic L_0 minimization approach proposed by Trzasko and Manduca [21] based on finite differential sparsifying transform. These methods are configured as presented in the respective research literature, as such configurations provided the best results based on testing. Note that the classic L_1 minimization approach and the homotopic L_0 minimization approach used for comparison purposes are effective at producing accurate reconstructions at higher k-space sampling rates. However, the goal here is to illustrate whether the proposed reconstruction approach is capable of producing more accurate reconstructions at sampling rates lower than existing approaches, thus facilitating lower breast MRI acquisition times. For example, since the acquisition time is proportional to the number of k-space lines acquired, a 83% k-space undersampling results in almost a 6:1 acquisition time acceleration. Given our previous example of approximately 14.5 minutes to acquire a sequence of 432 slices, given a time of repetition (TR) of 4.6ms and 420 TRs per slice, the reduced acquisition time would be approximately 2.4 minutes. This is by no means an exhaustive study of sparse MRI reconstruction methods, but does examine the performance of the proposed approach compared to a baseline method (L_2 minimization), a classic method (L_1 minimization with

total variation norm), and the method we wish to improve upon (homotopic L_0 minimization based on finite differential sparsifying transform).

Given that the proposed regional differential sparsifying transform can be considered a special case of the non-local total variation regularization framework where only close neighboring sites are used, we had also investigated the reconstruction accuracy of the non-local total variation approach using a searching window with width of 11 and patch size of 5×5 as specified in [14] under the homotopic L_0 framework. Note that the use of non-local total variation within the homotopic L_0 framework has not been previously explored in previous literature and can be considered a contribution of this work. Testing showed that the resulting reconstructions using both the regional differential sparsifying transform and the non-local total variation approach were very similar (with a SNR deviation of under 0.15 dB), which makes sense since the proposed regional differential sparsifying transform can be considered a special case of the non-local total variation approach. Since little performance gain was obtained by employing the non-local total variation framework over the proposed transform, both visually and quantitatively, only the results of the proposed regional differential sparsifying transform have been included.

For the L_1 minimization approach with total variation norm, homotopic L_0 minimization approach proposed by Trzasko and Manduca [21] based on finite differential sparsifying transform and the proposed approach, an iterative nonlinear diagonal normalized steepest descent solver [28] is used to compute the reconstructions, as employed in the homotopic L_0 framework proposed in [21]. While many different numerical optimization strategies [33], [34], [36], [37] can be used to solve for $\hat{f}(s)$, this fixed point iterative solver is simple to implement, has high computational efficiency, and provides accurate reconstructions based on testing as well as in previous literature [21]. A full description and implementation details of the solver can be found in [21]. For the sake of consistency, the parameters (e.g., λ , maximum number of iterations n_{\max} , etc.) pertaining to the solver used for all tested approaches are set to be the same as that presented in [21], with the exception of the maximum number of iterations for the proposed approach being set to $n_{\max} = 30$.

There are two important aspects that needs to be discussed when implementing the proposed approach: i) the objective function gradient used in the solver, and ii) the handling of boundary conditions. Given the objective function Υ presented in Eq. (11), the objective function gradient $\partial\Upsilon/\partial\hat{f}(s)$ can be derived as follows. Let Φ_F be the combined measurement-Fourier operator defined as

$$\Phi_F = \Phi\mathcal{F}, \quad (12)$$

For the real-value objective function defined in Eq. (10), the objective function gradient $\partial\Upsilon/\partial\hat{f}$ can be defined as

$$\frac{\partial\Upsilon}{\partial\hat{f}} = [\Psi_R^* J_{\hat{f}} \Psi_R + \lambda \Phi_F^* \Phi_F] \hat{f} - \lambda \Phi_F^* \Phi_F f, \quad (13)$$

with $J_{\hat{f}}$ defined as

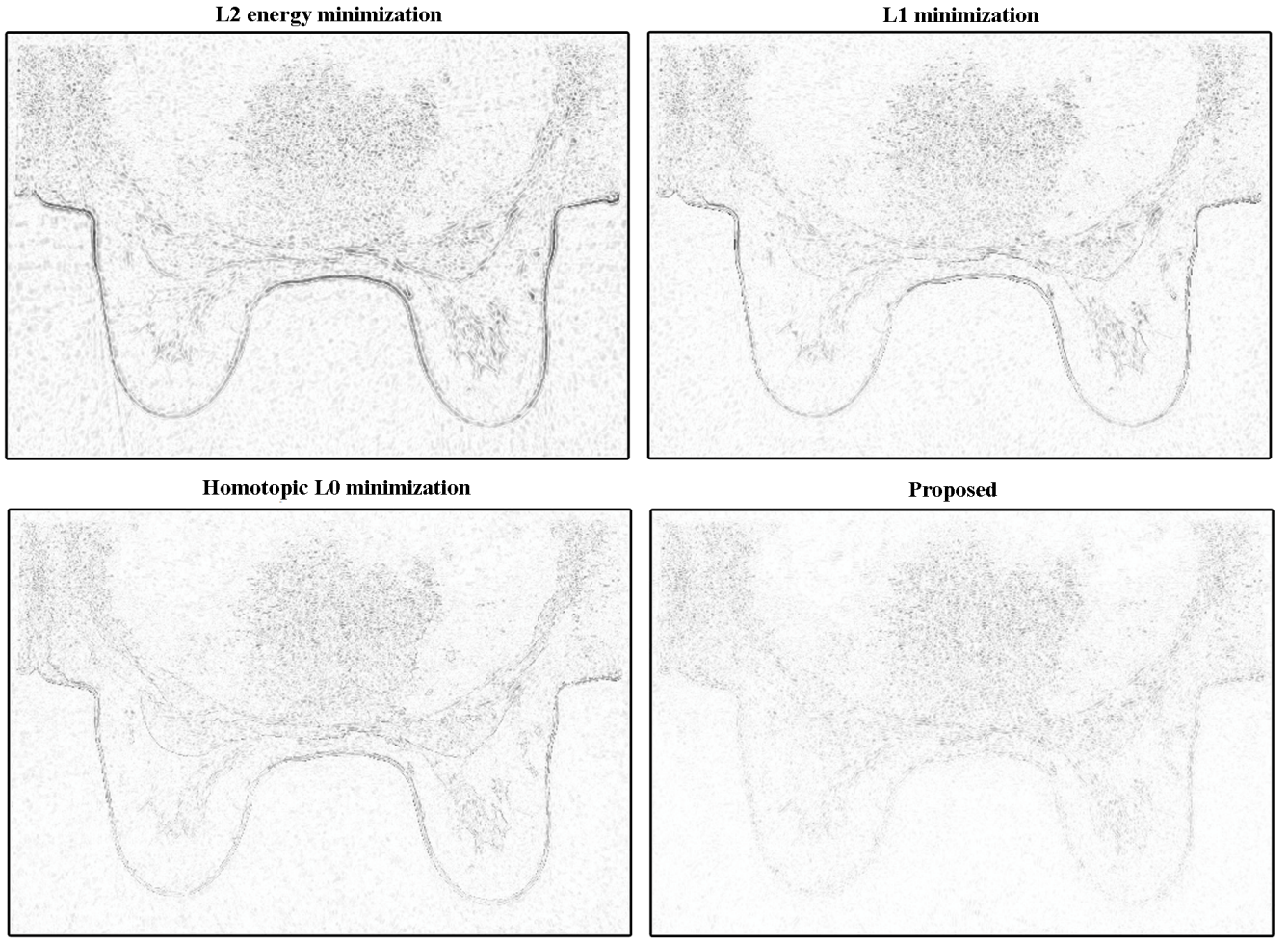


Fig. 5. Error maps for the first set of sample reconstructions using the tested breast MRI reconstruction methods.

$$\mathbf{J}_{\hat{f}} = \mathbf{I}_{n \times n} \otimes \mathbf{J}_{\hat{f}}^{\Gamma}, \quad (14)$$

where \otimes denotes the Kronecker product operator, $\mathbf{I}_{n \times n}$ is an $n \times n$ identity matrix, n is the number of sites within a fifth-order Markov connectivity around a central site, and $\mathbf{J}_{\hat{f}}^{\Gamma}$ is a diagonal matrix with its diagonal elements given by

$$\mathbf{J}_{\hat{f}}^{\Gamma}(s, s) = \frac{\rho' \left(\left| \Psi_R \hat{f}(s) \right|, \sigma \right)}{\left| \Psi_R \hat{f}(s) \right|}. \quad (15)$$

However, since we are dealing with complex-valued data, we wish to determine the objective function gradient for Eq. (11), which penalizes sparsity for both the real and imaginary components. Differentiating Υ as defined in Eq. (11) with respect to \hat{f} to obtain the objective function gradient yields the following Cauchy-Riemann system,

$$\left[\Psi_R^* \mathbf{J}_{\Re\{\hat{f}\}} \Psi_R + \lambda \Phi_F^* \Phi_F \right] \Re\{\hat{f}\} + i \left(\lambda \Phi_F^* \Phi_F \hat{f} \right) - \lambda \Phi_F^* \Phi_F f = 0, \quad (16)$$

and

$$\lambda \Phi_F^* \Phi_F \hat{f} + i \left(\left[\Psi_R^* \mathbf{J}_{\Im\{\hat{f}\}} \Psi_R + \lambda \Phi_F^* \Phi_F \right] \Im\{\hat{f}\} \right) - \lambda \Phi_F^* \Phi_F f = 0. \quad (17)$$

Given that the system defined by Eqs. (16) and (17) is under-determined, we instead compute the least squares estimate of the objective function gradient, which is defined by

$$\frac{\partial \Upsilon}{\partial \hat{f}} = \begin{aligned} & \left[\Psi_R^* \mathbf{J}_{\Re\{\hat{f}\}} \Psi_R + \lambda \Phi_F^* \Phi_F \right] \Re\{\hat{f}\} \\ & + i \left(\left[\Psi_R^* \mathbf{J}_{\Im\{\hat{f}\}} \Psi_R + \lambda \Phi_F^* \Phi_F \right] \Im\{\hat{f}\} \right) \\ & + \lambda \Phi_F^* \Phi_F \hat{f} - 2\lambda \Phi_F^* \Phi_F f. \end{aligned} \quad (18)$$

When employing the proposed sparsifying transform, the boundary conditions are handled in the following manner. First, for a site s under consideration, the regional difference with all neighbors that lie entirely outside the boundaries are treated as having a zero-value. Second, in the case where a region around the site s under consideration is entirely inside the boundaries but whose neighbors may lie partially outside the boundaries, the regional difference with all neighbors that lie partially outside of the boundaries is computed such that the sites within the neighbor's region falling outside the boundaries are treated as having a zero-value. Third, in the

case where the region around s itself lies partially outside the boundaries, then the sites within the region around s falling outside the boundaries are treated as having a zero-value.

The tested approaches were implemented in MATLAB and tested on an Intel Pentium 4 3.0 GHz machine with 1 GB of RAM. Each breast MRI slice took approximately 1 min to reconstruct using both the proposed approach and the homotopic L_0 minimization approach based on finite differential sparsifying transform (each iteration of the proposed approach took longer to compute, but the proposed approach required less iterations), 50 seconds for the L_1 minimization with total variation norm, and 17 minutes using the non-local total variation approach, which is not optimal for widespread clinical deployment but can be improved significantly through optimized code (since MATLAB is not well-suited for clinical deployment) and parallel processing paradigms. For the regional differential sparsifying transform, R is defined as 5×5 regions, as testing using breast MRI has shown little improvement in reconstruction accuracy when using regions larger than 5×5 . Finally, as with [21], the homotopic approximate of the L_0 norm was chosen as the Geman-McClure function [25],

$$\rho(|\Psi_R f(s)|, \sigma) = \frac{|\Psi_R f(s)|}{|\Psi_R f(s)| + \sigma}. \quad (19)$$

Two techniques were used to compare the different methods. To maintain consistency with other MRI reconstruction literature [10], [21], a visual assessment of the tested MRI reconstruction methods for sparse breast MRI reconstructions is performed. Furthermore, to investigate the reconstruction accuracy with respect to the number of samples used, the average signal to noise ratio (SNR) across the tested sets of breast MRI data was computed for various levels of undersampling. The SNR measured was computed according to the formula [38],

$$SNR(\hat{f}) = 10 \log_{10} \left(\frac{Var(f)}{Var(\hat{f} - f)} \right), \quad (20)$$

where $Var(f)$ is the variance of the reference data, and $Var(\hat{f} - f)$ is the error variance. The SNR measure indicates in a quantitative manner the reconstruction accuracy compared to the reference data, where a high SNR value indicates higher reconstruction accuracy.

The average SNR of the proposed approach compared to the other published methods as a function of percentage undersampling is demonstrated in Fig. 6. The average SNR decreases as the undersampling percentage increases for all tested methods. However, the proposed approach produces reconstructions with higher average SNR when compared to the other tested methods for all levels of undersampling percentage. An important insight that can be drawn from average SNR as a function of percentage undersampling is that the proposed approach is capable of producing accurate reconstructions using fewer samples than the other tested methods, which will reduce acquisition time and increase the total number of screenings that can be done as well as potentially reducing patient discomfort.

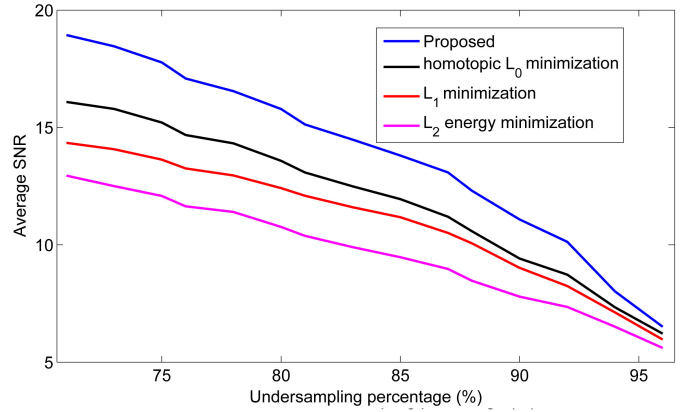


Fig. 6. Parametric test to illustrate the effect of percentage undersampling on average signal to noise ratio (SNR)

Sample reconstructions for two slices of the breast MRI data are shown in Figs. 1 and 3, with zoomed-in regions shown in Figs. 2 and 4. Note that the reconstructions shown in Figs. 1 and 3 are cropped versions of the reconstructions (which are square), and as such have non-square dimensions. The reconstruction produced by the L_2 energy minimization approach is contaminated by significant artifacts and possesses a blurred appearance. While the L_1 minimization approach performs well at significantly reducing such artifacts, the produced reconstruction still exhibits noticeable blurring in most areas. The homotopic L_0 minimization approach based on finite differential sparsifying transform produced reconstructions with minimal artifacts, and appears significantly sharper and higher contrast than the L_2 approach. However, the produced reconstruction exhibits noticeable staircase effects, which is particularly noticeable in the vessels in Fig. 2 and the circular mass and outer breast boundary in Fig. 4, producing a “cartoon”-like appearance with some loss of the finer details and signal variations.

Finally, the proposed approach is able to produce sharp and high contrast reconstructions that have minimal artifacts, good preservation of fine details and signal variations, as well as without any of the staircase artifacts exhibited by the homotopic L_0 minimization approach based on finite differential sparsifying transform. An error map for the first set of sample reconstructions is shown in Fig. 4. The reconstruction proposed by the proposed reconstruction approach exhibits noticeably lower reconstruction errors, particularly in the structured regions, when compared to the other tested methods.

IV. CONCLUSIONS

A novel approach for sparse reconstruction of a breast MR image using homotopic L_0 minimization based on the regional differential sparsifying domain was proposed and implemented. The effectiveness of the proposed approach in producing high contrast and sharp reconstructions that preserves finer structures characteristic of breast MRI while alleviating artifacts compared to other published methods is demonstrated.

Future work involve performing a comprehensive analysis of the performance of the proposed approach using more realistic cases with actual radial acquisitions, as well as for other types of medical imagery.

ACKNOWLEDGMENT

The authors would like to thank the Natural Sciences and Engineering Research Council (NSERC) of Canada and Geomatics for Informed Decisions (GEOIDE) for funding this project. The authors would also like to thank Sentinelle Medical Inc. for providing the breast MRI data used for testing.

REFERENCES

- [1] P. Boyle and B. Levin, "Breast Cancer," *World Cancer Report 2008*, IARC Press, pp. 412–417, 2008.
- [2] World Health Organization, "Fact sheet No. 297: Cancer," <http://www.who.int/mediacentre/factsheets/fs297/en/index.html>, Retrieved Oct. 4, 2009.
- [3] American Cancer Society, "Breast Cancer Facts & Figures 2009-2010," http://www.cancer.org/downloads/STT/F861009_final209-08-09.pdf, Retrieved Oct. 4, 2009.
- [4] P. Boyle and B. Levin, "Screening for Breast Cancer," *World Cancer Report 2008*, IARC Press, pp. 296–301, 2008.
- [5] W. Kaiser and E. Zeitler, "MR imaging of the breast: fast imaging sequences with and without Gd- DTPA. Preliminary observations", *Radiology*, vol. 170, pp. 681-686, 1989.
- [6] M. Bazzocchi, C. Zuiani, P. Panizza, C. Del Frate, F. Soldano, M. Isola, F. Sardanelli, G. Giuseppetti, G. Simonetti, V. Lattanzio, and A. Del Maschio, "Contrast-Enhanced Breast MRI in Patients with Suspicious Microcalcifications on Mammography: Results of a Multicenter Trial," *American Journal of Roentgenology*, vol. 186, pp. 1723-1732, 2006.
- [7] P. Mansfield, "Multi-planar image formation using NMR spin echos," *Journal of Physics C: Solid State Physics*, vol. 10, no. 3, pp. L55-L58, 1977.
- [8] E. Candés, J. Romberg, and T. Tao, "Robust uncertainty principles: exact signal reconstruction from highly incomplete frequency information," *IEEE Trans. Information Theory*, vol. 52, no. 2, pp. 489-509, 2006.
- [9] D. Donoho, "Compressed sensing," *IEEE Trans. Information Theory*, vol. 52, no. 4, pp. 1289-1306, 2006.
- [10] M. Lustig, D. Donoho, and J. Pauly, "Sparse MRI: The application of compressed sensing for rapid MR imaging," *Magnetic Resonance in Medicine*, vol. 58, no. 6, pp. 1182-1195, 2007.
- [11] K. Block, M. Uecker, and J. Frahm, "Undersampled radial MRI with multiple channels: iterative image reconstruction using a total variation constraint," *Magn. Reson. Med.*, vol. 57, pp. 1086-1098, 2007.
- [12] B. Liu, F. Seibert, Y. Zou, and L. Ying, "SparseSENSE: randomly-sampled parallel imaging using compressed sensing," *Proceedings of the 16th Annual Meeting of ISMRM*, 2008.
- [13] D. Liang, K. King, B. Liu, and L. Ying, "Accelerated SENSE using distributed compressed sensing," *Proceedings of the 17th Annual Meeting of ISMRM*, 2009.
- [14] D. Liang, H. Wang, and L. Ying, "SENSE Reconstruction with Nonlocal TV Regularization," *Proc. IEEE Eng. Med. Biol. Soc.* pp. 1032-1035, 2009.
- [15] D. Liang, B. Liu, J. Wang, and L. Ying, "Accelerating SENSE using compressed sensing," *Magnetic Resonance in Medicine*, vol. 62, no. 6, pp. 1574-1584, 2009.
- [16] H. Jung, K. Sung, K. Nayak, E. Kim, and J. Ye, "k-t FOCUSS: A general compressed sensing framework for high resolution dynamic MRI," *Magnetic Resonance in Medicine*, vol. 61, pp. 103-116, 2009.
- [17] Y. Kim, S. Narayanan, K. Nayak, "Accelerated Three-Dimensional Upper Airway MRI Using Compressed Sensing," *Magnetic Resonance in Medicine*, vol. 61, pp. 1434-1440, 2009.
- [18] R. Chartrand, "Fast algorithms for nonconvex compressive sensing: MRI reconstruction from very few data," *Proc. IEEE International Symposium on Biomedical Imaging (ISBI)*, 2009.
- [19] W. Lu and N. Vaswani, "Modified Compressive Sensing for Real-time Dynamic MR Imaging," *IEEE international conference on Image Processing*, 2009.
- [20] E. Candés, M. Wakin, and S. Boyd, "Enhancing Sparsity by Reweighted l_1 Minimization," *J. Fourier Anal. Appl.*, vol. 14, pp. 877-905, 2007.
- [21] J. Trzasko and A. Manduca, "Highly undersampled magnetic resonance image reconstruction via homotopic L_0 -minimization," *IEEE Trans. Medical Imaging*, vol. 28, no. 1, pp. 106-121, 2009.
- [22] S. Kindermann, S. Osher, and P. Jones, "Deblurring and denoising of images by nonlocal functionals," *SIAM MMS*, vol. 4, no. 4, pp. 1091-1115, 2005.
- [23] G. Gilboa and S. Osher, "Nonlocal operators with applications to image processing", *Multiscale Model. Simul.*, vol. 7, pp. 1005-1028, 2008.
- [24] A. Buades, B. Coll, and J. Morel, "Nonlocal image and movie denoising", *International Journal of Computer Vision*, vol. 76, no. 2, pp. 123140, 2008.
- [25] S. Geman and D. McClure, "Statistical methods for tomographic image reconstruction," *Bulletin of the International Statistical Institute*, LII-4, pp. 521, 1987.
- [26] L. Rudin, S. Osher, and E. Fatemi, "Non-linear total variation noise removal algorithm," *Phys. D*, vol. 60, pp. 259268, 1992.
- [27] E. Hendrick, *Breast MRI: Fundamentals and Technical Aspects*, Springer: New York, 2008.
- [28] D. Bertsekas, *Nonlinear Programming*, Belmont, MA: Athena, 1995.
- [29] G. Glover and J. Pauly, "Projection reconstruction technique for reduction of motion effects in MRI," *Magnetic Resonance in Medicine*, vol. 28, pp. 275-289, 1992.
- [30] K. Scheffler and J. Hennig, "Reduced circular field-of-view imaging," *Magnetic Resonance in Medicine*, vol. 40, no. 3, pp. 474-480, 1998.
- [31] J. Jackson, C. Meyer, D. Nishimura, A. Macovski, "Selection fo a convolution function for Fourier inversion using gridding", *IEEE Trans. Med. Imaging*, vol. 10, no. 3, pp. 473-478, 1991.
- [32] L. Sha, H. Guo, and A. Song, "An improved gridding method for spiral MRI using nonuniform fast Fourier transform," *Journal of Magnetic Resonance*, vol. 162, no. 2, pp. 250-258, 2003.
- [33] J. Ye, S. Tak, Y. Han, and H. Park, "Projection reconstruction MR imaging using FOCUSS," *Magnetic Resonance in Medicine*, vol. 57, pp. 764-775, 2007.
- [34] H. Jung, J. Ye, and E. Kim, "Improved k-t BLAST and k-t SENSE using FOCUSS," *Physics in Medicine and Biology*, vol. 52, pp. 3201-3226, 2007.
- [35] D. Noll, D. Nishimura, and A. Macovski, "Homodyne detection in magnetic resonance imaging," *IEEE Trans. Medical Imaging*, vol. 10, no. 2, pp. 154-163, 1991.
- [36] M. Figueiredo, R. Nowak, and S. Wright, "Gradient projection for sparse reconstruction: application to compressed sensing and other inverse problems", *IEEE Journal on Selected Topics in Signal Processing*, vol. 1, no. 4, pp. 586-597, 2007.
- [37] S. Kim, K. Koh, M. Lustig, and S. Boyd, "An interior-point method for large-scale L_1 -regularized least squares", *IEEE Journal on Selected Topics in Signal Processing*, vol. 1, no. 4, pp. 606-617, 2007.
- [38] A. Pizurica, W. Philips, I. Lemahieu, and M. Acheroy, "A versatile wavelet domain noise filtration technique for medical imaging," *IEEE Trans. Med. Imaging*, vol. 22, no. 3, pp. 323-331, 2003.